LITHOS 430-431 (2022) 106877

Contents lists available at ScienceDirect

LITHOS

journal homepage: www.elsevier.com/locate/lithos

Revisiting the origin of the Carboniferous Oytag pluton in West Kunlun orogenic belt, northwest China

Yan-Jun Wang [a,b], Wei-Guang Zhu [b,*], Hui-Qing Huang [c], Zheng-Wei Zhang [b,*], Peng-Cheng Hu [b], Cheng-Quan Wu [b], Jin-Hong Xu [b], Cheng-Biao Leng [a]

[a] State Key Laboratory of Nuclear Resources and Environment, East China University of Technology, Nanchang 330013, China
[b] State Key Laboratory of Ore Deposit Geochemistry, Institute of Geochemistry, Chinese Academy of Sciences, 99 West Lincheng Road, Guiyang 550081, China
[c] Economic Geology Research Center, College of Science and Engineering, Division of Tropical Environments and Societies, James Cook University, Townsville, QLD 4811, Australia

ARTICLE INFO

Keywords:
Oytag pluton
West Kunlun orogenic belt
Zircon trace elements
Paleo-Tethys Ocean

ABSTRACT

The Oytag pluton in the West Kunlun orogenic belt of China represents the rare exposed Carboniferous granitoids associated with the early-stage evolution of the Paleo-Tethys Ocean, and its origin is controversial. New zircon U-Pb data suggest an emplacement age of 327–324 Ma for trondhjemite, which slightly predated tonalite (~314 Ma). These results, along with available published ages, indicate several episodes of magmatism to build the Oytag pluton. Both trondhjemite and tonalite have positive whole-rock Nd isotopic compositions ($\varepsilon_{Nd}(t) = +4.56$ to +8.01 for trondhjemite; $\varepsilon_{Nd}(t) = +4.68$ to +6.15 for tonalite), which positively correlate with whole-rock MgO values. Given the presence of Ordovician inherited zircon grains, variations of whole-rock Nd isotopic compositions are attributed to addition of <10% crustal contaminants during assimilation and fractional crystallization (AFC) processes. Interestingly, trondhjemite and tonalite follow distinct AFC trends, consistent with their different ages.

Zircons from two trondhjemite samples have overlapping U-Pb ages but show distinctly different trace elements and internal structures (sector-zoned vs. oscillatory-zoned). The sector-zoned zircons have a less evolved signature of lower Hf contents, higher Eu/Eu* and Th/U ratios than the oscillatory-zoned ones, indicating significant crystal fractionation processes for their parental melts. The more variable Hf contents of the oscillatory-zoned zircons than those of the sector-zoned ones reflect a more dynamic environment where they crystallized. We propose that the sector-zoned zircons were crystallized from locked, interstitial melt in a mush and the oscillatory-zoned zircons from extracted melt. In situ crystal-liquid segregation in a mush chamber thereby could be an efficient approach to the differentiation of Oytag trondhjemite. On the other hand, zircons from tonalite have similar Hf contents to the sector-zoned zircons from trondhjemite, but display slightly higher Eu/Eu* ratios and much higher Th/U ratios. This indicates that tonalite should have experienced much different AFC processes from trondhjemite.

Both the episodic magmatism feature and the distinct differentiation processes argue for rises of different batches of magmatism to generate trondhjemite and tonalite in Oytag. Along with the large variations of Hf isotopes (5–6 epsilon units) in zircons, we propose a partial melting of juvenile mafic crust model for the Oytag pluton. Heat from upwelling of asthenosphere may have triggered the partial melting of wet, mafic underplates during the opening of a Paleo-Tethyan back-arc basin.

1. Introduction

Controversy on the generation of silicic magmatic rocks involves two competing paradigms (Moyen et al., 2021): the basaltic magma fractionation paradigm and the crustal melting paradigm. The former paradigm proposes that granitoids commonly have a mafic parental magma from mantle which could undergo differentiation and assimilation to form mafic-intermediate cumulate precursors or complementary products (e.g., Annen et al., 2006; Hildreth and Moorbath, 1988; Lee and Bachmann, 2014); whereas the latter paradigm revolves around

* Corresponding authors.
E-mail addresses: zhuweiguang@vip.gyig.ac.cn (W.-G. Zhu), zhangzhengwei@mail.gyig.ac.cn (Z.-W. Zhang).

https://doi.org/10.1016/j.lithos.2022.106877
Received 30 March 2022; Received in revised form 10 September 2022; Accepted 10 September 2022
Available online 15 September 2022

progressively partial melting of crustal material to arise different small batches of magmas to build a pluton (e.g., Collins et al., 2020a; Weinberg and Hasalova, 2015).

In the basaltic magma fractionation paradigm, a granitic magma is regarded as a long-lived mush system which is kept at high crystallinity and could undergo phase separation and formation of cumulate layers (e.g., Bachmann and Huber, 2019; Holness, 2018; Huber et al., 2009; Koyaguchi and Kaneko, 1999). Attempts of linking the genetic relationship between erupted, silicic volcanic and intruding crystal-rich, plutonic rocks reach a remarkable conclusion that the crystal-poor rhyolites and crystal-rich granite batholiths form the separated but complementary parts of the same mush system (Bachmann et al., 2007; Bachmann and Bergantz, 2004, 2008; Colombini et al., 2011; Gelman et al., 2014; Miller et al., 2005). Recently, it has been demonstrated that extracted melt in the "crystal mush model" could generate not only erupted volcanics but also frozen rhyolitic liquids as granites within a large silicic chamber (e.g., Schaen et al., 2017). For instance, the Nyemo composite pluton in the Gangdese batholith records a snapshot of melt extraction process in a silicic magmatic system, which generated the high-silica miarolitic and rapakivi granites as frozen, fractionated melt with monzogranites left behind as complementary silicic cumulates (Lu et al., 2022).

In the crustal melting paradigm, inputs of heat and fluids result in an anatectic lower crust that gives rise of leaked, individual batches of magmas to progressively form a pluton (Collins et al., 2020a; Moyen et al., 2021). Differentiation of these magmas is considered to be achieved through progressive segregation of residual minerals during melting (Collins et al., 2020a) or evolution in magma chambers (Wang et al., 2021). Huge batholith accumulated by multiple intrusions can be generated during a long interval of ca. 10 Myr (Coleman et al., 2004). A remarkable recognition in this paradigm is that the significant heterogeneous Hf isotopes in zircon of granitoids are caused by either disequilibrium melting of crustal rocks (Tang et al., 2014) or preferential dissolution of uranium-rich zircon in melting crustal source (Gao et al., 2022). The initial disequilibrium signature may be homogenized to some extent during shallow crustal level processes (Wang et al., 2021). Both these two paradigms were developed from substantial robust evidence and are logically legitimate, Moyen et al. (2021), however, emphasized that "the key question is not so much 'which' model applies, but 'where, when and to which extent'".

Uncertainty remains concerning the exact origin of the Carboniferous Oytag pluton in West Kunlun orogenic belt, northwest China. Previous investigations have invoked the aforementioned two competing paradigms (Moyen et al., 2021) for the Oytag pluton including the extreme differentiation of arc tholeiitic magmas (Ji et al., 2018; Jiang et al., 2008) and the partial melting of juvenile, basaltic crust (Kang et al., 2015; Zhang et al., 2006). Noteworthily, compositional diversity of different types of rocks (e.g., trondhjemite and tonalite) within the Oytag pluton was used as key evidence to support either the extensive fractionation model (Jiang et al., 2008) or the evident differentiation trend, albeit to a less extent, in the crustal melting model (Zhang et al., 2006). These interpretations implicitly assume that trondhjemite and tonalite were products of the same magmatic event. Even though numbers of high-quality geochronological data have been obtained for the Oytag pluton (Jiang et al., 2008; Kang et al., 2015; Li et al., 2009; Zhang et al., 2006), they primarily focus on zircons from trondhjemite samples. As a matter of fact, the only available zircon U-Pb ages for Oytag tonalite (Ji et al., 2018) are somehow ~10 Myr younger than those of trondhjemite. This raises the possibility that trondhjemite and tonalite may be generated by different episodes of magmatism, which is critical for our understanding of the origin of the Oytag pluton and thereby deserves further verification.

In this contribution, we present new zircon U-Pb geochronological data for both trondhjemite and tonalite from the Oytag pluton to test whether trondhjemite and tonalite were emplaced simultaneously. New whole-rock Sm-Nd isotopes along with available data from previous studies are used to provide insights into the shallow crustal level AFC processes. In addition, zircon trace elements and accompanying internal structure are employed to discuss the possible crystal-melt separation process during differentiation within a shallow crustal level mush chamber.

2. Geological setting and petrography

The West Kunlun orogenic belt represents the westernmost segment of the Central Orogenic Belt of China and is located between the Tibetan Plateau to the south and the Tarim Block to the north (Fig. 1a). There exist four NW–SE-striking sutures that separate five different terranes. From north to south these sutures and terranes are the North Kunlun Terrane (margin of Tarim Block), the Oytag–Kudi Suture, the South Kunlun Terrane, the Mazha–Kangxiwa Suture, the Tashkurghan–Tianshuihai Terrane, the Hongshanhu–Qiaoertianshan–Jinsha jiang Suture, the Karakoram Terrane, the Bangonghu–Nujiang Suture, and the Kohistan Terrane (Jiang et al., 2008; Liu et al., 2015). The South Kunlun Terrane was believed to contain a post-Archean Precambrian metamorphic basement (Yuan et al., 2002) that is similar to that of the Tarim Block. This terrane was thought to be a southern extension of Tarim block and was split during the late Neoproterozoic opening of the Proto-Tethyan Ocean (Matte et al., 1996). The South Kunlun Terrane records the early Paleozoic southward subduction of Proto-Tethyan oceanic crust (Mattern and Schneider, 2000; Yuan et al., 2005), an event that formed a 506–405 Ma granitoid belt within the terrane (Fig. 1b). The final closure of the Proto-Tethyan Ocean at Middle Silurian resulted in continental collision of the South Kunlun Terrane and the Tarim Block (Yuan et al., 2002), generating the Oytag–Kudi Suture (Jia et al., 2013; Liu et al., 2014).

The Tashkurghan–Tianshuihai Terrane is located to the south of the South Kunlun Terrane and contains the Tianshuihai Group as Precambrian basement with a covering Paleozoic–Mesozoic sedimentary sequence (Zhang et al., 2019). The Paleo-Tethys Ocean had separated the South Kunlun Terrane and the Tashkurghan–Tianshuihai Terrane before the Early Carboniferous (ca. 338 Ma; Jiang et al., 2013). The majority of the Paleo-Tethyan oceanic crustal subduction has a northward subduction polarity beneath the South Kunlun Terrane (Bi et al., 1999). This caused sporadic but coeval granitoid and mafic magmatism within the South Kunlun Terrane (Ji et al., 2018; Li et al., 2006; Liu et al., 2015). The exact timing of the collision between the South Kunlun Terrane and the Tashkurghan–Tianshuihai Terrane is highly controversial but is likely to have occurred between the Late Permian and the Late Triassic–Late Jurassic (Jiang et al., 2013; Mattern and Schneider, 2000; Xiao et al., 2005). Nevertheless, it is generally accepted that the Mazha–Kangxiwa Suture marks the final closure of the Paleo-Tethys Ocean, an event that involved the generation of voluminous Triassic granitoids (Fig. 1b).

The Oytag pluton, together with the Saluoyi pluton to the northwest, represent the rare exposed, late Carboniferous felsic magmatism in the South Kunlun Terrane. The Oytag pluton crops out over an area of ~60 km^2 (Zhang et al., 2006). It intruded into the Mesoproterozoic Saitula Group and the Late Carboniferous Wuluate Formation and is locally covered by lower Permian sedimentary units (Fig. 1c). The Saitula Group contains Precambrian metamorphosed volcanic and clastic rocks, whereas the Wuluate Formation consists of a volcanic-sedimentary sequence that is dominated by mafic lavas with minor amounts of felsic volcanic layers and thin-bedded limestones (Ji et al., 2018). The basaltic lavas of the Wuluate Formation are divided into a lower part that is interbedded with radiolarian-bearing chert and an upper part containing andesite and dacite lavas (Deng, 1995). The volcanic rocks within this formation are characterized by pillowed basalts, suggesting a submarine environment (Ji et al., 2018). Some gabbro stocks also intruded into the Wuluate Formation. There are east–west-striking dolerite dikes that range in width from tens of centimeters to several meters (Ji et al., 2018). They crosscut the Oytag basalts, gabbros, and

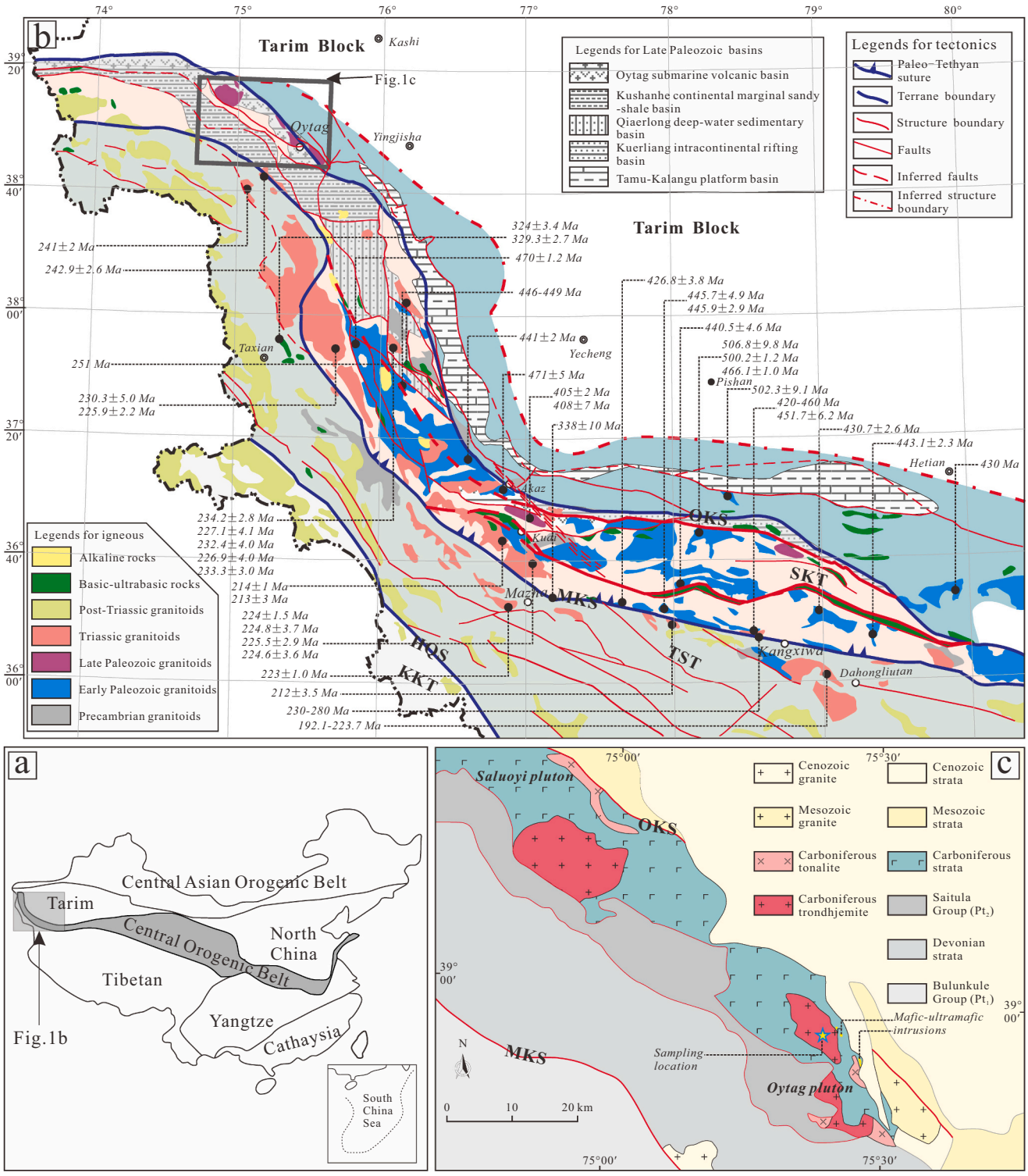

Fig. 1. (a) The tectonic framework of China. (b) Simplified geological map of the western part of the West Kunlun orogenic belt, NW China. (c) Geological map of the Oytag area showing the locations of the Oytag pluton and the Saluoyi pluton (modified after Kang et al., 2015). Abbreviations: HQS = Hongshanhu–Qiaoertianshan–Jinshajiang Suture, KKT = Karakoram Terrane, MKS = Mazha–Kangxiwa Suture, OKS = Oytag–Kudi Suture, TST = Tashkurghan–Tianshuihai Terrane, and SKT = South Kunlun Terrane. The ages shown in b are compiled from previously published studies (e.g., Jiang et al., 2013; Liu et al., 2015; Zhang et al., 2006; Zhang et al., 2016 and references therein).

the felsic pluton (Fig. 2) and extend for tens to hundreds of meters along strike.

The Oytag felsic pluton comprises a suit of low-K felsic rocks, including trondhjemite and tonalite. Early studies named these low-K rocks as "plagiogranite" and considered them to be the felsic part of "the Oytag ophiolite" (e.g., Jiang et al., 1992), the westerly equivalent of the 510 ± 4 Ma Kudi ophiolite (e.g., Pan and Wang, 1994). Admittedly, the Oytag felsic pluton shares many geochemical characteristics (e.g., flat REE patterns and positive Nd isotopic compositions) with oceanic plagiogranites (e.g., Zhang et al., 2006). However, available zircon U-Pb

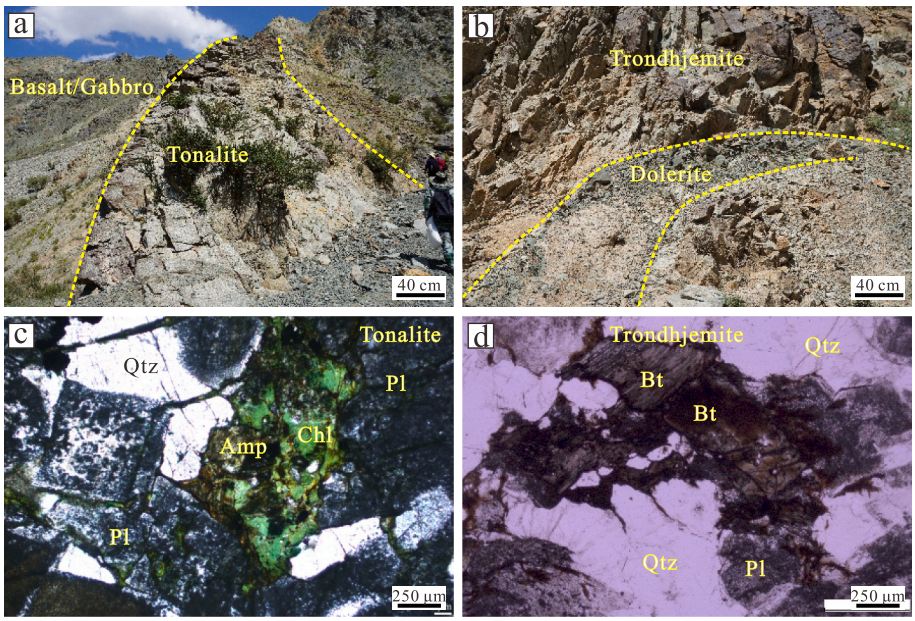

Fig. 2. Field photographs showing Oytag tonalite intruding the basaltic lavas and gabbros (a) and Oytag trondhjemite intruded by dolerite dike (b). Photomicrographs of representative tonalite (c) and trondhjemite (d). Abbreviations: Amp = amphibole; Bt = biotite; Chl = chlorite; Pl = plagioclase; and Qtz = Quartz.

data from the Oytag felsic pluton yield Carboniferous ages (340 Ma to 314 Ma; Zhang et al., 2006; Jiang et al., 2008; Li et al., 2009; Ji et al., 2018; this study), arguing against that the genetic connection between the Kudi ophiolite and the so-called "Oytag ophiolite" (e.g., Zhang et al., 2006). Indeed, no convincing evidence has been reported to support the presence of "Oytag ophiolite". Importantly, the Oytag felsic low-K rocks

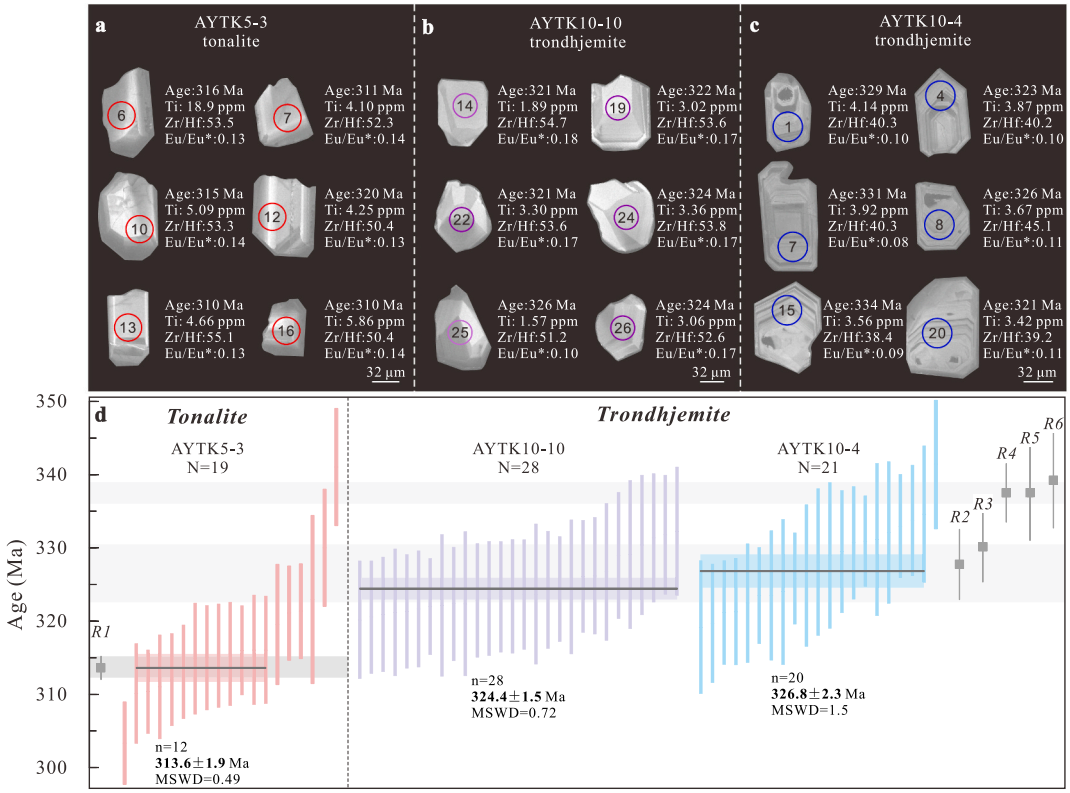

Fig. 3. Representative cathodoluminescence images of zircon grains used for LA-ICP-MS U-Pb dating for tonalite and trondhjemite samples (a–c). LA-ICP-MS zircon $^{206}Pb/^{238}U$ ages (d) for the Oytag pluton. Note that zircons from trondhjemite AYTK10–10 show much different structures from those of trondhjemite AYTK10–4. An Ordovician inherited zircon grain (~440 Ma) is not shown in Fig. 3a due to the scale limit. Circles in a–c represent the 32 μm spot used for U-Pb dating; ages and key chemical indices are also shown for analyzed zircon grains. $^{206}Pb/^{238}U$ ages in Fig. 3d are plotted as averages with two-standard-error intervals (2σ); n represents analyses used for the calculation of weighted mean age, while N represents the total number of analyses for each sample. Available geochronological data from previous studies are also shown for comparison. Several younger zircon grains from tonalite sample in Ji et al. (2018) have been excluded from plotting. Data sources include Ji et al. (2018) (R1), Jiang et al. (2008) (R2 and R4), Zhang et al. (2006) (R3) and Li et al. (2009) (R5 and R6).

form a large-sized pluton (~60 km^2; Zhang et al., 2006), differing from the classic, vein-like oceanic plagiogranites in ophiolite and oceanic mid-ridge (e.g., Chen et al., 2019). To avoid misunderstanding, we would refrain from using the terminology of "plagiogranite" to describe the Oytag pluton in the following discussion.

This study collected 17 samples from the Oytag pluton. Oytag tonalite is gray and contains 60%–65% plagioclase, 20%–25% quartz, and 10%–15% amphibole. In contrast, Oytag trondhjemite is grayish white and contains less plagioclase (53%–58%), more quartz (30%–40%) and biotite (~10%). Both tonalite and trondhjemite contain variable amounts of accessory Fe-Ti oxides, apatite, and zircon. Analysis of the minerals indicates that the plagioclase is albite and that the amphibole is classified as ferro- to magnesio-hornblende (Jiang et al., 2008), which corresponds to pressure of ~92 MPa (3.2–3.5 km), and water contents of ~6.7% by Al-in-hornblende thermobarometer (Ridolfi et al., 2010). These rocks have undergone variable degrees of alteration with plagioclase locally altered to sericite and amphibole and biotite partly replaced by epidote and chlorite (Fig. 2c–d).

3. Analytical results

Analytical methods used in this study are provided in the Supplementary Material.

3.1. Zircon U-Pb dating

Geochronological data for analyzed Oytag trondhjemite and tonalite samples are summarized in Supp. Table 1 and shown in Fig. 3. Tonalite sample AYTK5–3 contains euhedral zircons with weakly oscillatory zoning in CL images (Fig. 3a). The majority of these zircons are 60–140 μm long with length-to-width ratios of 1.2–2.0. They contain 170–737 ppm U and 108–1311 ppm Th with Th/U ratios of 0.63 to 1.70. One dark zircon grain (spot 18) yields a $^{206}Pb/^{238}U$ age (440 ± 4 Ma) much older than the rest of the zircons analyzed from this sample. Another six analyses (spots 1, 9, 12, 15, 19 and 20) have $^{206}Pb/^{238}U$ ages of 341–320 Ma, which are slightly older than the majority of the zircons in these samples (314 Ma; Fig. 3d). One zircon grain (spot 17) has a young $^{206}Pb/^{238}U$ age of 303 Ma. The remaining 12 analyses have $^{206}Pb/^{238}U$ age of 310 Ma to 316 Ma, yielding a weighted mean age of 313.6 ± 1.9 Ma (2σ, MSWD = 0.49; Fig. 3d), which represents the crystallization age of sample AYTK5–3.

Zircons extracted from trondhjemite sample AYTK10–10 are sector-zoned, subhedral-euhedral crystals which are 70–130 μm long with length-to-width ratios of 1.0–1.5 (Fig. 3b). The sector-zoned feature has been confirmed by zircons from the thin slice of AYTK10–10 (Fig. S1a–d). A total of 28 analyses indicate that these zircons contain 83.7–236 ppm U and 35.9–181 ppm Th, yielding Th/U ratios of 0.37–0.77. All 28 analyses have $^{206}Pb/^{238}U$ ages spanning from 320 Ma to 332 Ma with a weighted mean age of 324.4 ± 1.5 Ma (2σ, MSWD = 0.72; Fig. 3d), which represents the crystallization age of sample AYTK10–10.

Zircons extracted from trondhjemite sample AYTK10–4 are oscillatory-zoned, euhedral crystals in CL images (Fig. 3c). They are 60–160 μm long with length-to-width ratios of 1.2–2.5. The oscillatory-zoned feature has been confirmed by zircons from the thin slice of AYTK10–4 (Fig. S1e–h). A total of 21 analyses of these zircons indicate they contain 71.2–485 ppm U and 16.7–246 ppm Th, respectively, yielding Th/U ratios of 0.22–0.51. One analysis (spot 5) have a slightly older age of 341 Ma, which is not included in calculating weighted mean age for the sample; twenty analyses yield $^{206}Pb/^{238}U$ ages varying from 319 Ma to 335 Ma with a weighted mean age of 326.8 ± 2.3 Ma (2σ, MSWD = 1.5; Fig. 3d), which represents the timing of formation of sample AYTK10–4.

3.2. Whole-rock major and trace elements

Whole-rock major and trace elements of analyzed Oytag samples are given in Supp. Table 2. To extend dataset in this study, we also compile available whole-rock major and trace element data from previous studies (Ji et al., 2018; Jiang et al., 2008; Kang et al., 2015; Zhang et al., 2006). Oytag felsic samples are plotted within trondhjemite and tonalite fields as they are characterized by low K but high Na contents (Fig. 4a–c); they also show metaluminous and weakly peraluminous features (Fig. 4d). Tonalite samples have SiO_2 contents ranging from 56.2 wt% to 72.4 wt% (volatile free). Trondhjemite samples are chemically more evolved than tonalite with higher SiO_2 contents (72.3–79.2 wt%).

Oytag tonalite samples contain relatively low total rare-earth element (REE) contents (ΣREE = 46.4–73.7 ppm) and have nearly flat chondrite-normalized REE patterns ($(La/Yb)_N$ = 0.50–1.50) with variably Eu anomalies ($Eu/Eu^* = Eu_N/(Sm_N*Gd_N)^{0.5}$, N donates chondrite-normalization; Eu/Eu* = 0.38–1.26; Fig. 5a). They also show flat primitive mantle-normalized multi-element variation patterns with negative Nb-Ta-Sr-P-Ti and positive K anomalies (Fig. 5b). Compared with tonalite, trondhjemite samples have similar flat REE (ΣREE = 56.9–222 ppm; $(La/Yb)_N$ = 0.57–1.61; Eu/Eu* = 0.18–0.80) and multi-element variation patterns but show more negative Nb-Ta-Sr-P-Ti anomalies (Fig. 5c–d).

3.3. Whole-rock Sr-Nd isotopes and zircon Lu-Hf isotopes

Whole-rock Sr-Nd isotopic compositions of analyzed Oytag samples are given in Supp. Table 2. To extend dataset in this study, we compile available whole-rock Sr-Nd isotopic data from previous studies (Jiang et al., 2008; Zhang et al., 2006). Oytag tonalite samples have variable initial $^{87}Sr/^{86}Sr$ ratios (0.7039–0.7063) but a narrow range of initial $^{143}Nd/^{144}Nd$ values (0.51289–0.51299) that yield $\varepsilon_{Nd}(t)$ values of 4.68–6.15 (Fig. 6) and two-stage Nd model ages (T_{2DM}) of 0.52–0.35 Ga (Supp. Table 2). Trondhjemite samples have ranges of initial $^{87}Sr/^{86}Sr$ (0.7039–0.7068), initial $^{143}Nd/^{144}Nd$ (0.51288–0.51301), $\varepsilon_{Nd}(t)$ (4.56–8.01), and T_{2DM} (0.51–0.35 Ga) values (Fig. 6; Supp. Table 2).

Zircon Lu-Hf isotopic compositions of one tonalite sample and two trondhjemite samples are given in Supp. Table 3. Tonalite sample AYTK5–3 has positive zircon $\varepsilon_{Hf}(t)$ values (6.63–12.8) and young two-stage Hf model ages (0.67–0.34 Ga), except for one grain with significant lower $\varepsilon_{Hf}(t)$ value of 1.26 (Fig. 6b). Trondhjemite sample AYTK10–10 has highly positive zircon $\varepsilon_{Hf}(t)$ values of 10.1–15.5 (Fig. 6b) with two-stage Hf model ages of 0.69–0.35 Ga (Supp. Table 3). Trondhjemite sample AYTK10–4 has a similar range of zircon $\varepsilon_{Hf}(t)$ values (10.4–15.5) and two-stage Hf model ages (0.67–0.34 Ga) to that of sample AYTK10–10 (Fig. 6b; Supp. Table 3).

3.4. Zircon trace elements

Zircons from one tonalite sample and two trondhjemite samples have distinctly different trace element compositions (Fig. 7; Supp. Table 1). Zircons from trondhjemite sample AYTK10–10 have lower Hf contents (8987–9864 ppm), higher Eu/Eu* (0.10–0.20), Th/U (0.37–0.77), Sm/Yb (0.005–0.009), Nb/Ta (3.05–4.86) ratios, and REE contents (1840–5128 ppm) than those of trondhjemite sample AYTK10–4 (Hf = 10,638–13,179 ppm; Eu/Eu* = 0.04–0.13; Th/U = 0.22–0.51, Sm/Yb = 0.004–0.015, Nb/Ta = 2.33–4.31) ratios, and REE = 1181–4551). Compared with those of trondhjemite sample AYTK10–10, zircons from tonalite sample AYTK5–3 have similar Hf contents (8959–12,218 ppm), but lower Eu/Eu* ratios (0.06–0.14) and higher Th/U (0.63–1.70), Sm/Yb (0.006–0.014), Nb/Ta (3.65–6.86) ratios, and REE contents (2342–13,247).

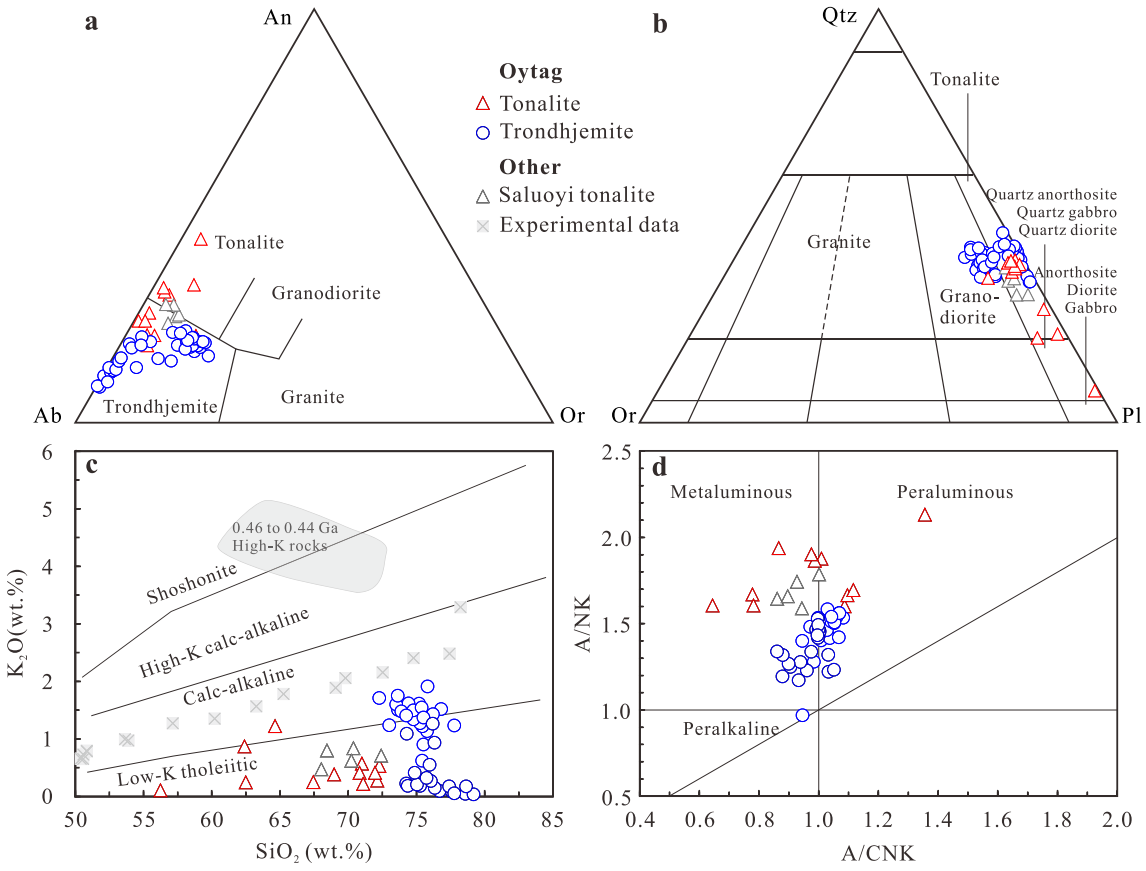

Fig. 4. Normative whole-rock anorthite (An)–albite (Ab)–orthoclase (Or) (a; Barker, 1979) and quartz (Qtz)–orthoclase (Or)–plagioclase (Pl) (b; Le Bas and Streckeisen, 1991) ternary diagrams for the Oytag pluton. Variations of K_2O vs. SiO_2 (c; Rickwood, 1989) and A/NK vs. A/CNK (d) for the Oytag pluton. A/NK = molar ratio of $Al_2O_3/(Na_2O + K_2O)$, A/CNK = molar ratio of $Al_2O_3/(CaO + Na_2O + K_2O)$. Data sources for the Oytag pluton are listed in Supp. Table 2. For the purpose of comparison, data of Saluoyi tonalite (Kang et al., 2015), Ordovician high-K granitoids (Wang et al., 2017) and experimentally fractional crystallization of medium-K magmas (Nandedkar et al., 2014) are shown in Fig. 4c.

4. Discussion

4.1. A multistage magmatic history for the Oytag pluton

Previous SHRIMP zircon U-Pb dating suggested the Oytag pluton was formed at 340–328 Ma (R2, R3, R4, R5 and R6 in Fig. 3d; Zhang et al., 2006; Jiang et al., 2008; Li et al., 2009). However, LA-ICP-MS method gave a remarkable younger age of 314 ± 2 Ma (R1 in Fig. 3d; Ji et al., 2018). Such an over 10 Myr gap may be resulted from different analytical methods or uncertainties. However, our new U-Pb data preclude this possibility as two distinct populations of zircon U-Pb ages were obtained using a single analytical method in this study (Fig. 3).

Our dating results indicate that Oytag trondhjemite was emplaced at 327 ± 2 Ma and 324 ± 2 Ma (Fig. 3d), confirming the previous ages of 328 ± 5 Ma (R2 in Fig. 3d; Jiang et al., 2008) and 330 ± 5 Ma (R3 in Fig. 3d; Zhang et al., 2006). In contrast, zircons from a tonalite were dated at 314 ± 2 Ma (AYTK5–3 in Fig. 3d), identical to the data reported by Ji et al., (2018). Mineralogical and geochemical examination confirms the tonalite affinities of the sample (R1) used for dating in Ji et al. (2018). This demonstrates that Oytag tonalite should form at 314 Ma with ~10 Myr later than Oytag trondhjemite.

Notably, some trondhjemite samples were determined with ages of ~338 Ma (R4, R5 and R6 in Fig. 3d; Jiang et al., 2008; Li et al., 2009), suggesting the onset of Oytag felsic magmatism. The activity of ~338 Ma felsic magmatism is additionally evidenced by sparse ~338 Ma zircons in the postdated rocks (Fig. 3d). Geologically, the ~338 Ma trondhjemite crops out as small intrusions, contrasting with the 330–324 Ma trondhjemite, which forms large intrusions (Jiang et al., 2008). These two episodes of trondhjemite, however, are indistinguishable in whole-rock geochemistry and Sr-Nd-Hf isotopes, as well as plagioclase chemistry (Jiang et al., 2008). For simplification, we will not make further efforts to distinguish them from each other. We thus propose that the Oytag pluton was built by several episodes of magmatism at ~338 Ma, 330–324 Ma and ~ 314 Ma (Fig. 3d).

4.2. Source of Oytag felsic magmas

Oytag samples show relatively variable Sr isotopic compositions that may be indicative of post-magmatic alteration (Jiang et al., 2008). In comparison, whole-rock Sm-Nd and zircon Lu-Hf isotopic systems are generally more resistant to alteration processes compared with Rb-Sr isotopic systems. Both Oytag trondhjemite and tonalite have highly radiogenic whole-rock Nd ($\varepsilon_{Nd}(t)$ = 4.56 to 8.01) and zircon Hf ($\varepsilon_{Hf}(t)$ = 6.63 to 15.5) isotopes, which suggest sources of either depleted mantle or juvenile mafic lower crust with a short crustal residence age. This precludes an ancient crustal sedimentary source, consistent with the absence of Al-rich minerals (e.g., tourmaline and peritectic garnet) in the Oytag pluton as well as its relatively low A/CNK feature (A/CNK ratios mostly <1.1).

Identification of some 480–440 Ma inherited zircons (this study and Jiang et al., 2008), however, indicates that minor Nd-Hf isotopically unradiogenic material should have been involved into the generation of the Oytag pluton. Given the high-K to extremely high-K nature, the 480–440 Ma felsic magmatic rocks (e.g., Wang et al., 2017) could not be sources for the low-K Oytag pluton. Possibility exists that the Ordovician rocks contaminated the magmas of the Oytag pluton in crustal level.

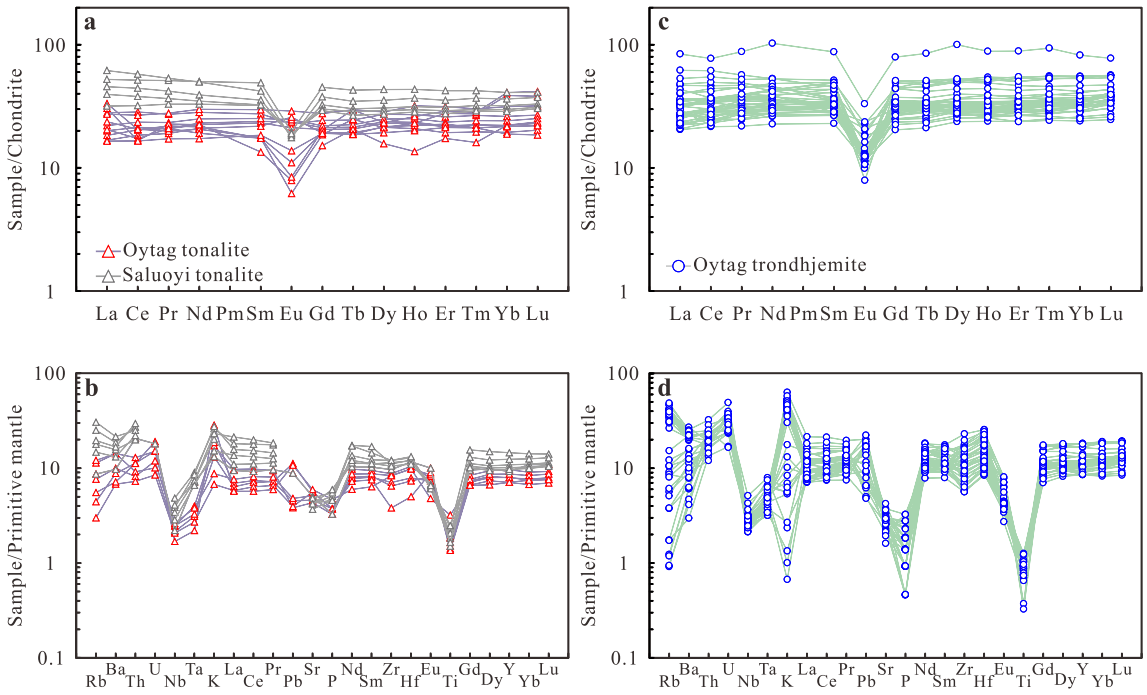

Fig. 5. Chondrite-normalized REE and primitive mantle-normalized multi-element variation diagrams for the Oytag pluton. Normalizing values of chondrite and primitive mantle come from Sun and McDonough (1989). Data of Saluoyi tonalite (Kang et al., 2015) are shown for comparison. Note that Oytag trondhjemite samples have consistent REE and multi-element patterns except for some mobile elements such as Rb, Ba and K.

Simple Nd-Hf isotopic mixing modeling using end-members of mid-ocean ridge basalt (MORB) and Ordovician rocks within the West Kunlun orogenic belt suggests that isotopic features of the Oytag pluton could be reproduced by depleted mantle-derived melts with participation of <10% material of 462–444 Ma granitoids in the region (Fig. 6b). Indeed, as shown in Fig. 6c–d, whole-rock $\varepsilon_{Nd}(t)$ values exhibit linearly relationships with whole-rock MgO and SiO_2 contents for both Oytag trondhjemite and tonalite. These observations are consistent with AFC processes during which crustal contamination has lowered the whole-rock $\varepsilon_{Nd}(t)$ values of the relatively evolved samples from the Oytag pluton. The least-evolved samples from the Oytag pluton provide better constraints on chemical characteristics of their sources. The least-evolved Oytag trondhjemite and tonalite have whole-rock $\varepsilon_{Nd}(t)$ values slightly more enriched than that of MORB (Fig. 6a–b). Such a moderately depleted Nd isotopic signature is a common feature as well as shared by the Carboniferous mafic rocks in Oytag (Fig. 6a, c–b). Specially, available Oytag gabboric samples, which were believed to have not been significantly changed by crustal level contamination, display a narrow $\varepsilon_{Nd}(t)$ range of 6.01–6.69 (n = 5; Ji et al., 2018), confirming the moderately depleted nature for melting mantle sources beneath Oytag. Because Oytag gabbros have zircon U-Pb ages (~330 Ma; unpublished data) overlapping that of the neighboring Oytag felsic pluton, we propose that sources for the Oytag pluton may have moderately depleted Sm-Nd isotopes comparable with that of gabbros. In this scenario, crustal contamination, albeit non-negligible, should be limited to an extent <10% during the generation of the Oytag pluton. We suggest that magmas of the Oytag pluton were mainly derived from Nd-Hf moderately depleted sources (mantle or juvenile crust).

4.3. Shallow crustal-level differentiation

4.3.1. Differentiation revealed by zircon trace elements

As aforementioned, AFC processes are necessary for not only the co-variation of whole-rock $\varepsilon_{Nd}(t)$ and MgO (or SiO_2) values of the Oytag felsic samples but also the presence of minor Ordovician inherited zircons from the Oytag pluton. Zircon trace elements provide important constraints on differentiation process of their parental melt. For instance, Hf contents and Zr/Hf ratios in zircon have been widely used as monitors to trace chemical evolution of parental melt (Claiborne et al., 2006, 2010; Deering et al., 2016; Schaen et al., 2017; Yan et al., 2018, 2020). To be specific, more evolved melts would precipitate zircon with higher Hf and lower Zr/Hf. For Oytag trondhjemite, zircons from trondhjemite AYTK10–4 display a more evolved signature with higher Hf contents, and lower Zr/Hf, Eu/Eu*, Th/U, Sm/Yb and Nb/Ta ratios, as well as lower REE contents than those of trondhjemite AYTK10–4 (Fig. 7), consistent with a higher degree of differentiation. It is highly likely that zircon grains from these two trondhjemite samples precipitated from melts with variable degrees of fractional crystallization. Fractionating mineral assemblage of plagioclase, biotite (± quartz) and apatite/monazite/titanite resembling that of trondhjemite could account for the chemical evolution trend (Fig. 7). Predominant plagioclase and biotite fractionation could generate coupling decreases in Eu/Eu* (Trail et al., 2012) and Nb/Ta ratios (Ballouard et al., 2020). In addition, LREE-bearing minerals (e.g., apatite, titanite and monazite) saturation is evidenced by decreasing REE contents and Sm/Yb ratio (Fig. 7d–e). Monazite saturation could contribute to the decreasing Th/U during competition with zircon (Harrison et al., 2007). We also note that fractionation of titanite, a mineral that preferentially incorporates Ta over Nb (Ballouard et al., 2020) and Hf over Zr (Bea et al., 2006), may have buffered the decreasing trends of Nb/Ta and Zr/Hf, but its effect should be limited due to a relatively limited volume (<0.1%) during fractionation.

Except for several grains with slightly older, trondhjemite-like ages, most of zircon grains from tonalite also show variable Hf contents (Fig. 7). Given the highly variable REE contents and Sm/Yb and Th/U ratios, it is likely that tonalite zircons could have been precipitated from gradually evolving melts. However, it is worthy to note that tonalite zircon grains record an evolving trend distinctly different from the one defined by trondhjemite zircons. Significantly, the relatively constant Eu/Eu* ratios for most of zircon grains of tonalite are inconsistent with massive plagioclase fractionation. Instead, LREE-bearing minerals (e.g., monazite) could have played a significant role in fractionating mineral

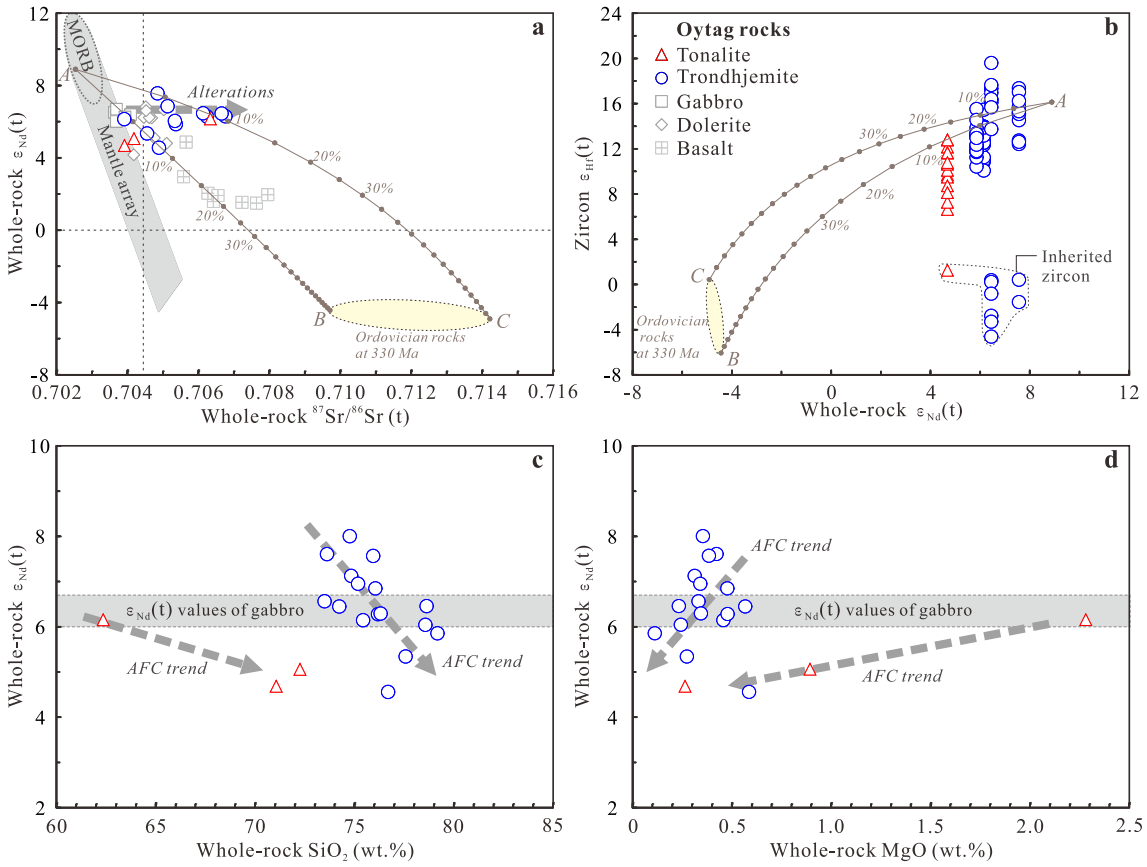

Fig. 6. Diagrams showing variations of whole-rock $\varepsilon_{Nd}(t)$ vs. whole-rock $(^{87}Sr/^{86}Sr)_i$ (a), zircon $\varepsilon_{Hf}(t)$ vs. whole-rock $\varepsilon_{Nd}(t)$ (b), whole-rock $\varepsilon_{Nd}(t)$ vs. whole-rock SiO_2 (c), and whole-rock $\varepsilon_{Nd}(t)$ vs. whole-rock MgO (d) for the Oytag pluton. Sr-Nd isotopic data of Oytag gabbro, dolerite and basalt come from Ji et al. (2018). Binary mixing curves between depleted mantle-derived melt and Ordovician granitoids are also shown in Fig. 6a–b. End-member A (MORB) has Sr = 136 ppm, Nd = 8 ppm, Hf = 2.5 ppm, $^{87}Sr/^{86}Sr = 0.70263$, $^{143}Nd/^{144}Nd = 0.51313$, and $^{176}Hf/^{177}Hf = 0.28326$ (Chauvel and Blichert-Toft, 2001; Workman and Hart, 2005), whereas end-members B (Sr = 759 ppm, $^{87}Sr/^{86}Sr = 0.71122$, Nd = 42.3 ppm, $^{143}Nd/^{144}Nd = 0.51222$, Hf = 4.9 ppm, and $^{176}Hf/^{177}Hf = 0.28241$) and C (Sr = 719 ppm, $^{87}Sr/^{86}Sr = 0.71653$, Nd = 19 ppm, $^{143}Nd/^{144}Nd = 0.51219$, Hf = 1.8 ppm, and $^{176}Hf/^{177}Hf = 0.28259$) are Ordovician granitoids (Wang et al., 2017). Each tick represents 5% increment of contamination. Note that the inherited zircons of the Oytag pluton have Lu-Hf compositions identical to the Ordovician granitoids. AFC represents assimilation and fractional crystallization processes.

assemblage. This finding is consistent with the observation that Oytag tonalite follows a different AFC trend from trondhjemite in the whole-rock $\varepsilon_{Nd}(t)$ and MgO (or SiO_2) diagram.

4.3.2. Crystal-liquid segregation

The Oytag pluton is characterized by high SiO_2 (mostly >70 wt%). Application of Al-in-hornblende barometry (Ridolfi et al., 2010) suggests emplacement at 3.2–3.5 km depth for Oytag tonalite (Jiang et al., 2008), consistent with the common shallow crustal origin (<10 km) for high-silica granites (>70 wt% SiO_2; Lee and Morton, 2015). High-silica rocks are generally hypothesized to represent interstitial melt separated from large, upper crustal, crystal-rich mush chambers via crystal-liquid segregation (i.e., fractionation) (Bachmann and Bergantz, 2004; Gualda and Ghiorso, 2014; Lee and Morton, 2015). It is worthy to test if the crystal-liquid segregation process is recorded by Oytag felsic samples.

Zircon internal structure together with accompanying trace elements could provide critical constraints on crystal-liquid segregation process within silicic magma reservoirs. For example, Lu et al. (2022) identified two types of zircons from Nyemo composite pluton including the bright Type A zircons and the dark Type B zircons, corresponding to less-evolved and more-evolved compositions, respectively. Type A zircons were proposed to be captured during melt extraction event from crystal mush, while Type B zircons were considered to crystallize subsequent to the melt extraction event (Lu et al., 2022). In the case of Oytag, we also recognized two types of zircons from trondhjemite including the sector-zoned zircons from sample AYTK10–10 and the oscillatory-zoned zircons from sample AYTK10–4 (Fig. 3). Oscillatory bands indicate pronounced kinetic factors that affect the distribution of trace elements within zircon (e.g., Zou et al., 2021). In contrast, the occurrence of sector zoning of zircons from intrusive igneous rocks is a natural consequence simply of slow lattice diffusion, which does not require equilibrium-limiting kinetic process (e.g., Watson and Liang, 1995). We propose that the sector-zoned zircons (sample AYTK10–10) were precipitated from locked, interstitial melt and oscillatory-zoned zircons (sample AYTK10–4) from less-locked melt. Constant, low Hf values of sector-zoned zircons (sample AYTK10–10; less-evolved) contrast with the variable and elevated Hf values of oscillatory-zoned zircons (sample AYTK10–4; more-evolved) (Fig. 8). We consider that the oscillatory-zoned zircons were generated in a more dynamic environment, maybe the extracted melt, than sector-zoned zircons within a common trondhjemitic mush chamber (Fig. 9). Kinetic processes may have complicated the effort to rebuild the relationship between melt chemistry and zircon composition due to disequilibrium. However, much larger beam spot sizes in LA-ICP-MS analysis than the width of oscillatory bands within zircon have erased the significant heterogeneity. As a matter of fact, the obtained zircon trace elements for oscillatory-zoned zircon follow the chemical trends modeled by Rayleigh fractionation (Fig. 8). We thus propose that the two types of zircon from Oytag trondhjemite record in situ differentiation via crystal-liquid segregation.

Zircon from Oytag tonalite generally has identical internal structure

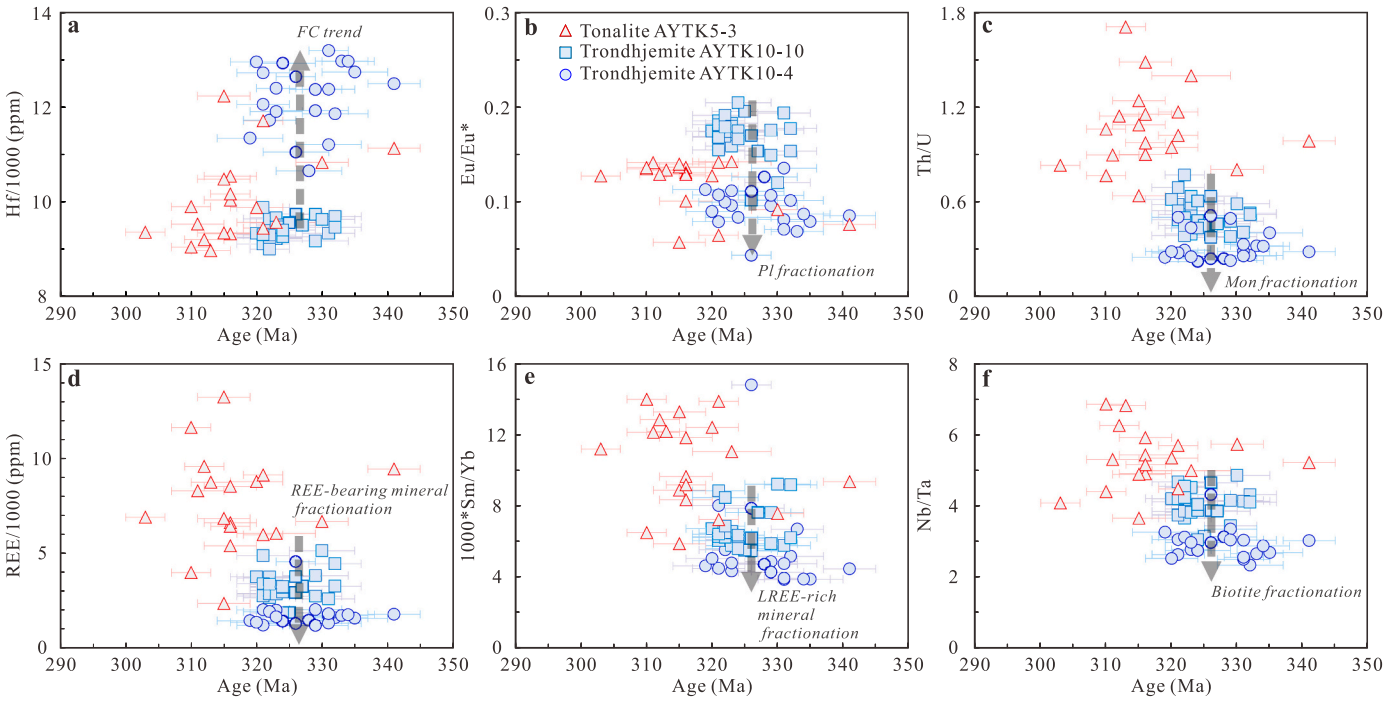

Fig. 7. Diagrams showing variations of Hf contents, Eu/Eu* and Th/U ratios, REE contents, and Sm/Yb and Nb/Ta ratios vs. U-Pb ages for the Oytag pluton. Each spot is plotted with $^{206}Pb/^{238}U$ age at one-standard-error interval (1σ). Eu/Eu* = $Eu_N/(Sm_N*Gd_N)^{0.5}$, N donates chondrite-normalization; FC = fractional crystallization; LREE = light rare earth element; Mon = monazite; Pl = plagioclase. Note the variations of trace elements between the sector-zoned zircons of trondhjemite AYTK10–10 and the oscillatory-zoned zircons of trondhjemite AYTK10–4 are consistent with crystal fractionation processes.

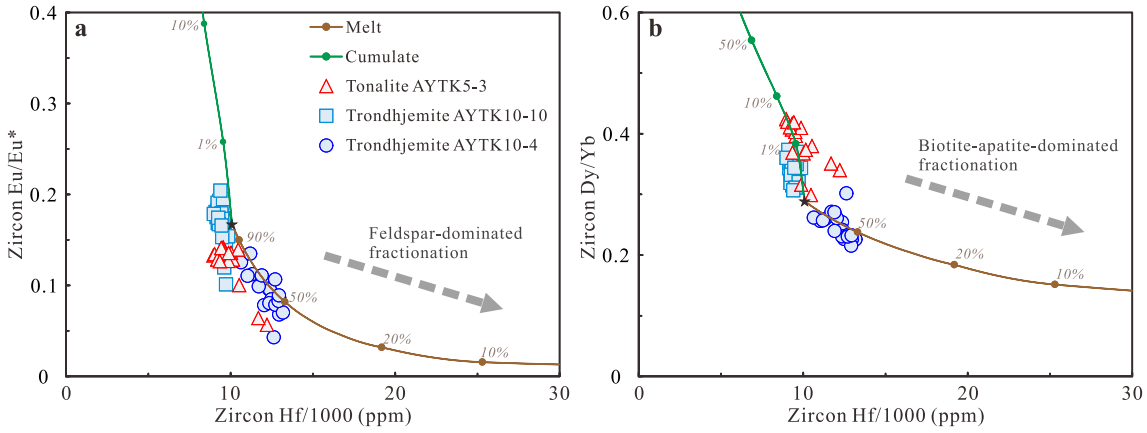

Fig. 8. Plots of Eu/Eu* vs. Hf/1000 (a) and Dy/Yb vs. Hf/1000 (a) for zircons from the Oytag pluton. Dashed arrows indicate fractionation trends that could account for the co-variations of Eu/Eu*, Dy/Yb and Hf/1000. Rayleigh fractional crystallization modeling used the 1:1 mixing compositions of zircon samples AYTK10–10-27 and AYTK10–4-9 as the starting point (black stars). Details are provided in the Supp. Table 4.

(Fig. 3a). Crystal-liquid segregation within Oytag tonalite could not be identified due to the limited amounts of zircon data. Nevertheless, it could be precluded that Oytag tonalite is the cumulate phase left after trondhjemite melt extraction given their distinctly different zircon U-Pb ages and differentiation trends.

4.4. Mantle or crust model for the Oytag pluton?

Experiment results confirmed that SiO_2-rich magmas could be produced though extensive differentiation of mantle-derived, hydrous, basaltic magmas within a wide temperature range of 1170–700 °C (e.g., Nandedkar et al., 2014). The continuous variations of whole-rock major elements from mafic dikes via tonalite to trondhjemite in Oytag have led Jiang et al. (2008) to infer that the felsic rocks were highly differentiated products of the mafic end-member. They further precluded the crustal partial melting model by presenting a REE modeling. Interestingly, a totally opposite result from similar REE modeling was obtained to support the crustal partial melting model (Zhang et al., 2006). This discrepancy is caused by the different partition coefficients and residual minerals adopted in modeling. Despite the weakness of previous REE modeling, this study provides several lines of evidence supporting the crustal partial melting model.

(1) New geochronological data demonstrate that tonalite formed ~10 Myr later than trondhjemite in Oytag, indicating that tonalite and trondhjemite could not be generated in a single magmatic event. Any attempt to rebuild the geochemical evolution from tonalite to trondhjemite is inappropriate. As demonstrated above, tonalite and trondhjemite actually follow distinctly different evolution trends in both AFC

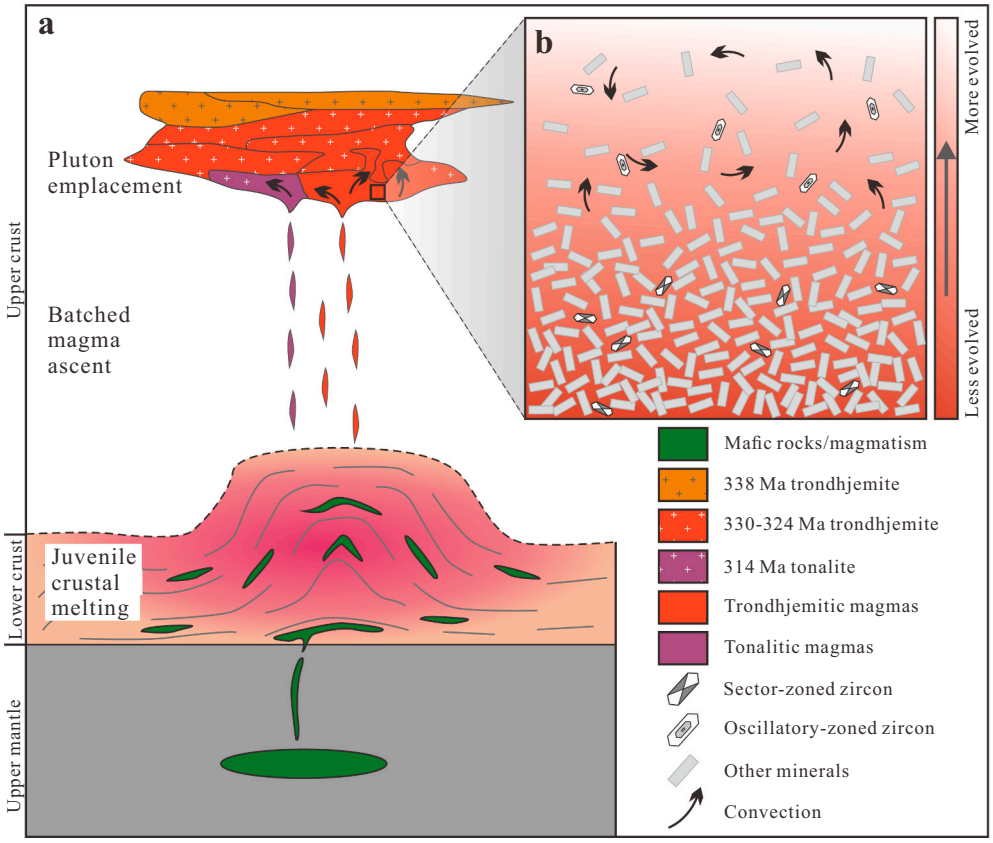

Fig. 9. Schematic diagram of the crustal melting model for the Oytag pluton (modified after Moyen et al., 2021). Different batches of felsic magmas were leached from the ductile, melting lower crust and then transferred to stack in upper crust, thereby generating the episodic features of the Oytag pluton. For the 330–324 Ma trondhjemite, differentiation via in situ crystal-liquid segregation could account for the AFC processes and the growth of coeval zircons with contrasting structures.

processes and zircon compositions. These observations are inconsistent with the extensive fractionation model. Rather, the episodic pattern for the Oytag pluton is similar to the incremental assembly processes of the huge Tuolumne Intrusive Suite (Coleman et al., 2004).

(2) Large variations (5–6 epsilon units) in zircon Hf isotopes for single specimen have been recognized in rocks from the Oytag pluton. The relatively constant 5–6 epsilon-unit variations in zircon Hf isotopes for samples with different degrees of contamination (Fig. 6) indicate that the hafnium isotopic heterogeneity for each sample is not a contamination result but an intrinsic feature of source melting. Crustal melting would result in such variations via disequilibrium melting (Tang et al., 2014) or preferential dissolution of uranium-rich zircon (Gao et al., 2022). We cannot confirm the feasibility of the dissolution of uranium-rich zircon model because the required high-U zircons are less common in juvenile mafic crustal sources than in metasedimentary sources. An evidence supporting this interpretation is that zircons from the Oytag pluton generally have U contents lower than 800 ppm, inconsistent with resultants of dissolution of uranium-rich zircon (Gao et al., 2022). Alternatively, we propose that presence of zircon grains, albeit minor, crystallized in mafic underplates, deep equivalents of the Oytag gabbros, may have amplified the Hf isotopic variations during disequilibrium melting.

(3) The Oytag pluton generally has high SiO_2 (>70 wt%). High-silica (>70 wt%) granites should represent <20% (Nandedkar et al., 2014) or at most 5% (Lee and Morton, 2015) of the original mass if they have a basaltic parent. Expectation for this process is that there should be large volumes of mafic-intermediate complementary cumulate for the extremely evolved felsic rocks. For example, oceanic plagiogranites that may form via fractional crystallization of basaltic magmas are volumetrically small veins (~0.5%) relative to the gabbroic section of Ocean Drilling Program Hole 735B within the Southwest Indian Ridge (Chen et al., 2019). However, ultramafic-mafic-intermediate cumulates comprise <5% of the area of outcrop in Oytag (Fig. 1c), unlike the oceanic ridge scenario. Instead, the dominance of silicic rocks in Oytag shows consistency with the Sierra Nevada batholith of California (Bateman and Chappell, 1979), where voluminous, juvenile, tonalitic magmas were also generated via fluid-fluxed melting (Collins et al., 2020a). We propose that parental magmas of the Oytag pluton were derived from partial melting of wet juvenile crust via reactions consuming quartz and plagioclase (Collins et al., 2020a; Conrad et al., 1988).

Geodynamic setting of the Oytag pluton was interpreted to be associated with either the Carboniferous continental rifting in northern margin of the Tarim block (Zhang et al., 2006) or an intra-oceanic subduction within the Paleo-Tethys Ocean between South Kunlun terrane and Tarim block (Jiang et al., 2008). However, a most recent study on mafic rocks in Oytag concluded that the Oytag mafic magmatism was generated in a back-arc basin at late Carboniferous (Ji et al., 2018). We concur with the back-arc geodynamic model given the evidence below (Fig. 10). Firstly, Oytag basalts and gabbros collectively display “arc-signatured” Nb-Ta negative anomalies, indicating significant addition of slab fluid/melt (Ji et al., 2018). Secondly, increasing Nd isotopic compositions from early basalts to late gabbros are consistent with attenuating arc signature for the melting mantle beneath Oytag (Ji et al., 2018). Thirdly, to the south of Oytag, the Mazha arc belt was found to be a response to the northward subduction and consumption of Paleo-Tethys since 338 Ma (Li et al., 2006). In addition, Carboniferous strata (e.g., Wuluate Formation and its lateral equivalents) in Oytag have abundant terrestrial detritus, consistent with deposition in back-arc basins (Ji et al., 2018). We thereby propose that heating-triggered partial melting of wet, mafic underplates during back-arc crustal thinning provides a plausible scenario for the generation of magmas for the

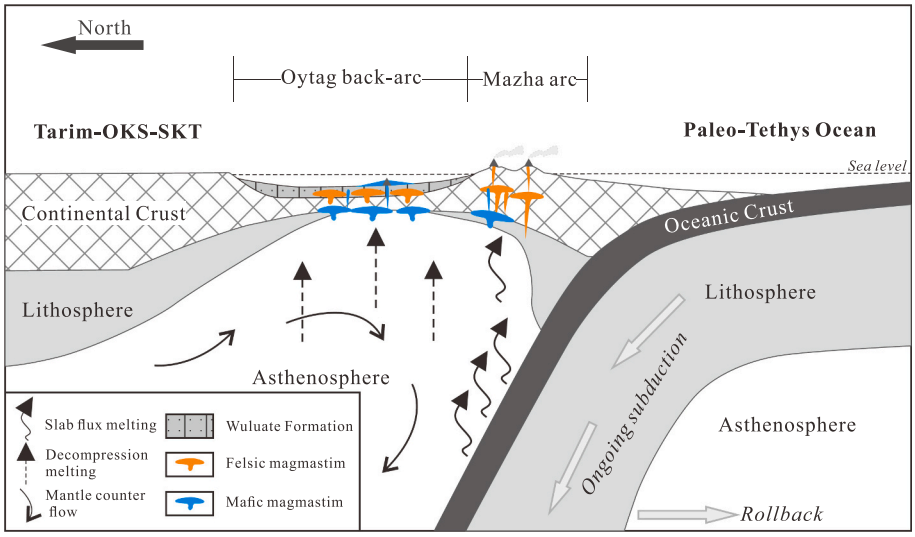

Fig. 10. Geodynamic model for the Oytag pluton. The diagram is modified from the model for I-type granites in the Lachlan orogen (Collins et al., 2020b).

Oytag felsic pluton.

5. Conclusions

(1) New geochronological data suggest that trondhjemite and tonalite were formed by different batches of magmas at 327–324 Ma and 314 Ma, respectively.

(2) Both whole-rock Nd isotopes and zircon trace elements indicate significant AFC processes in magma chambers for the Oytag pluton. AFC processes suggest that trondhjemite could not be directly evolved from parental magmas of tonalite.

(3) Differentiation within trondhjemite may be achieved by in situ crystal-liquid segregation.

(4) Parental magmas of the Oytag pluton were derived from partial melting of wet, juvenile mafic crust beneath a back-arc basin of the Paleo-Tethys Ocean.

Supplementary data to this article can be found online at https://doi.org/10.1016/j.lithos.2022.106877.

Declaration of Competing Interest

The authors declare that they have no known competing financial interests or personal relationships that may influence the work reported in this paper.

Acknowledgements

This study is financially supported by the National Natural Science Foundation of China (Grants U1603245, 41572074 and 42002210). Wang acknowledges the Open Project Fund from the State Key Laboratory of Ore Deposit Geochemistry, Institute of Geochemistry, Chinese Academy of Sciences (202212). We gratefully acknowledge Y.W., Chen for his guidance in LA-(MC)-ICP-MS zircon U-Pb and Lu-Hf isotopic analyses. Y.J., Wang thanks J., Hu and Y., Huang for their assistance in whole-rock trace element analyses. F. Xiao is specially appreciated for her timely whole-rock Sr-Nd isotopes separation and concentration prior to measurement. This paper benefits from the insightful comments from the editor Di-Cheng Zhu, the reviewer Peng Gao and an anonymous reviewer.

References

Annen, C., Blundy, J.D., Sparks, R.S.J., 2006. The genesis of intermediate and silicic magmas in deep crustal hot zones. Journal of Petrology 47, 505–539.

Bachmann, O., Bergantz, G.W., 2004. On the origin of crystal-poor rhyolites: extracted from batholithic crystal mushes. Journal of Petrology 45, 1565–1582.

Bachmann, O., Bergantz, G.W., 2008. Rhyolites and their source mushes across tectonic settings. Journal of Petrology 49 (12), 2277–2285.

Bachmann, O., Huber, C., 2019. The inner workings of crustal distillation columns; the physical mechanisms and rates controlling phase separation in silicic magma reservoirs. Journal of Petrology 60, 3–18.

Bachmann, O., Miller, C.F., De Silva, S., 2007. The volcanic–plutonic connection as a stage for understanding crustal magmatism. Journal of Volcanology and Geothermal Research 167, 1–23.

Ballouard, C., Massuyeau, M., Elburg, M.A., Tappe, S., Viljoen, F., Brandenburg, J.T., 2020. The magmatic and magmatic-hydrothermal evolution of felsic igneous rocks as seen through Nb-Ta geochemical fractionation, with implications for the origins of rare-metal mineralizations. Earth Science Reviews 203, 103115.

Barker, F., 1979. Trondhjemite: Definition, environment and hypotheses of origin. In: Barker, F. (Ed.), Developments in Petrology, vol. 6. Elsevier, Amsterdam, Netherlands, pp. 1–12.

Bateman, P.C., Chappell, B.W., 1979. Crystallization, fractionation, and solidification of the Tuolumne intrusive series, Yosemite National Park, California. Geological Society of America Bulletin 90, 465–482.

Bea, F., Montero, P., Ortega, M., 2006. A LA–ICP–MS evaluations of Zr reservoirs in common crustal rocks: implications for Zr and Hf geochemistry, and zircon-forming processes. The Canadian Mineralogist 44 (3), 693–714.

Bi, H., Wang, Z.G., Wang, Y.L., Zhu, X.Q., 1999. History of tectono-magmatic evolution in the Western Kunlun Orogen. Science in China Series D: Earth Sciences 42, 604–619.

Chauvel, C., Blichert-Toft, J., 2001. A hafnium isotope and trace element perspective on melting of the depleted mantle. Earth and Planetary Science Letters 190, 137–151.

Chen, Y.H., Niu, Y.L., Wang, X.H., Gong, H.M., Guo, P.Y., Gao, Y.J., Shen, F.Y., 2019. Petrogenesis of ODP Hole 735B (Leg 176) oceanic plagiogranite: Partial melting of gabbros or advanced extent of fractional crystallization? Geochemistry, Geophysics, Geosystems 20, 2717–2732.

Claiborne, L.L., Miller, C., Walker, B., Wooden, J., Mazdab, F., Bea, F., 2006. Tracking magmatic processes through Zr/Hf ratios in rocks and Hf and Ti zoning in zircons: an example from the Spirit Mountain batholith, Nevada. Mineralogical Magazine 70, 517–543.

Claiborne, L.L., Miller, C.F., Wooden, J.L., 2010. Trace element composition of igneous zircon: a thermal and compositional record of the accumulation and evolution of a large silicic batholith, Spirit Mountain, Nevada. Contributions to Mineralogy and Petrology 160, 511–531.

Coleman, D.S., Graym, W., Glazner, A.F., 2004. Rethinking the emplacement and evolution of zoned plutons: Geochronologic evidence for incremental assembly of the Tuolumne intrusive suite, California. Geology 32, 433–436. https://doi.org/10.1130/G20220.1.

Collins, W.J., Murphy, J.B., Johnson, T.E., Huang, H.Q., 2020a. Critical role of water in the formation of continental crust. Nature Geoscience 13, 331–338.

Collins, W.J., Huang, H.Q., Bowden, P., Kemp, A.I.S., 2020b. Repeated S–I–A-type granite trilogy in the Lachlan Orogen and geochemical contrasts with A-type granites in Nigeria: implications for petrogenesis and tectonic discrimination. In: Janousek, V., Bonin, B., Collins, W.J., Farina, F., Bowden, P. (Eds.), Post-Archean Granitic Rocks: Contrasting Petrogenetic Processes and Tectonic Environments, 491. Geological Society, London, Special Publications, pp. 53–76.

Colombini, L.L., Miller, C.F., Gualda, G.A., Wooden, J.L., Miller, J.S., 2011. Sphene and zircon in the Highland Range volcanic sequence (Miocene, southern Nevada, USA): elemental partitioning, phase relations, and influence on evolution of silicic magma. Mineralogy and Petrology 102, 29.

Conrad, W., Nicholls, I., Wall, V., 1988. Water-saturated and-undersaturated melting of metaluminous and peraluminous crustal compositions at 10 kb: evidence for the origin of silicic magmas in the Taupo Volcanic Zone, New Zealand, and other occurrences. Journal of Petrology 29, 765–803.
Deering, C.D., Keller, B., Schoene, B., Bachmann, O., Beane, R., Ovtcharova, M., 2016. Zircon record of the plutonic-volcanic connection and protracted rhyolite melt evolution. Geology 44, 267–270.
Deng, W.M., 1995. The geologic characteristics of the ophiolites in the Karakorum–West Kunlun region and their tectonic significance. Acta Petrologica Sinica 11 (S), 98–111 (in Chinese with English abstract).
Gao, P., Yakymchuk, C., Zhang, J., Yin, C.Q., Qian, J.H., Li, Y.G., 2022. Preferential dissolution of uranium-rich zircon can bias the hafnium isotope compositions of granites. Geology 50, 336–340. https://doi.org/10.1130/G49656.1.
Gelman, S.E., Deering, C.D., Bachmann, O., Huber, C., Gutierrez, F.J., 2014. Identifying the crystal graveyards remaining after large silicic eruptions. Earth and Planetary Science Letters 403, 299–306.
Gualda, G.A.R., Ghiorso, M.S., 2014. Phase-equilibrium geobarometers for silicic rocks based on rhyolite-MELTS. Part 1: principles, procedures, and evaluation of the method. Contributions to Mineralogy and Petrology 168, 1–17. https://doi.org/10.1007/s00410-014-1033-3.
Harrison, T.M., Watson, E.B., Aikman, A.B., 2007. Temperature spectra of zircon crystallization in plutonic rocks. Geology 35, 635–638.
Hildreth, W., Moorbath, S., 1988. Crustal contributions to arc magmatism in the Andes of central Chile. Contributions to Mineralogy and Petrology 98, 455–489.
Holness, M.B., 2018. Melt segregation from silicic crystal mushes: a critical appraisal of possible mechanisms and their microstructural record. Contributions to Mineralogy and Petrology 173, 48.
Huber, C., Bachmann, O., Manga, M., 2009. Homogenization processes in silicic magma chambers by stirring and mushification (latent heat buffering). Earth and Planetary Science Letters 283, 38–47.
Ji, W.H., Chen, S.J., Li, R.S., He, S.P., Zhao, Z.M., Pan, X.P., 2018. The origin of Carboniferous-Permian magmatic rocks in Oytag area, West Kunlun: Back-arc basin? Acta Petrologica Sinica 34 (8), 2393–2409 (in Chinese with English abstract).
Jiang, C.F., Yang, J.S., Feng, B.G., Zhu, Z., 1992. Opening–Closing Tectonics of the Kunlun Mountains. Geological Publishing House, Beijing.
Jiang, Y.H., Liao, S.Y., Yang, W.Z., Shen, W.Z., 2008. An island arc origin of plagiogranites at Oytag, western Kunlun orogen, northwest China: SHRIMP zircon U–Pb chronology, elemental and Sr–Nd–Hf isotopic geochemistry and Paleozoic tectonic implications. Lithos 106, 323–335.
Jiang, Y.H., Jia, R.Y., Liu, Z., Liao, S.Y., Zhao, P., Zhou, Q., 2013. Origin of Middle Triassic high-K calc-alkaline granitoids and their potassic microgranular enclaves from the western Kunlun orogen, northwest China: a record of the closure of Paleo-Tethys. Lithos 156–159, 13–30.
Jia, R.Y., Jiang, Y.H., Liu, Z., Zhao, P., Zhou, Q., 2013. Petrogenesis and tectonic implications of early Silurian high-K calc-alkaline granites and their potassic microgranular enclaves, western Kunlun orogen, NW Tibetan Plateau. International Geology Review 55, 958–975.
Kang, L., Xiao, P.X., Gao, X.F., Wang, C., Yang, Z.C., Xi, R.G., 2015. Geochemical characteristics, petrogenesis and tectonic setting of Oceanic plagiogranites belt in the northwestern margin of western Kunlun. Acta Petrologica Sinica 31 (9), 2566–2582.
Koyaguchi, T., Kaneko, K., 1999. A two-stage thermal evolution model of magmas in continental crust. Journal of Petrology 40, 241–254.
Le Bas, M.J., Streckeisen, A.L., 1991. The IUGS systematics of igneous rocks. Journal of the Geological Society 148 (5), 825–833.
Lee, C.T.A., Bachmann, O., 2014. How important is the role of crystal fractionation in making intermediate magmas? Insights from Zr and P systematics. Earth and Planetary Science Letters 393, 266–274.
Lee, C.T.A., Morton, D.M., 2015. High silica granites: Terminal porosity and crystal settling in shallow magma chambers. Earth and Planetary Science Letters 409, 23–31.
Li, B.Q., Yao, J.X., Ji, W.H., Zhang, J.L., Yin, Z.Y., Chen, G.C., Lin, X.W., Zhang, Q.S., Kong, W.N., Wang, F., Liu, X.P., 2006. Characteristics and zircon SHRIMP U–Pb ages of arc magmatic rocks in Mazar, southern Yecheng, West Kunlun Mountains. Geological Bulletin of China 25, 124–132 (in Chinese with English abstract).
Li, G.W., Fang, A.M., Wu, F.Y., Liu, X.H., Pan, Y.S., Wang, S.G., 2009. Studies on the U–Pb ages and Hf isotopes of zircons in the Aoyitake plagiclase granite, west Tarim. Acta Petrologica Sinica 25 (1), 166–172 (in Chinese with English abstract).
Liu, Z., Jiang, Y.H., Jia, R.Y., Zhao, P., Zhou, Q., Wang, G.C., Ni, C.Y., 2014. Origin of Middle Cambrian and Late Silurian potassic granitoids from the western Kunlun orogen, northwest China: a magmatic response to the Proto-Tethys evolution. Mineralogy and Petrology 108 (1), 91–110.
Liu, Z., Jiang, Y.H., Jia, R.Y., Zhao, P., Zhou, Q., 2015. Origin of Late Triassic high-K calcalkaline granitoids and their potassic microgranular enclaves from the western Tibet Plateau, northwest China: implications for Paleo-Tethys evolution. Gondwana Research 27, 326–341.
Lu, T.Y., He, Z.Y., Klemd, R., 2022. Identifying crystal accumulation and melt extraction during formation of high-silica granite. Geology 50 (2), 216–221. https://doi.org/10.1130/G49434.1.
Matte, Ph., Tapponnier, P., Arnaud, N., Bourjot, L., Avouac, J.P., Vidal, Ph., Liu, Q., Pan, Y.S., Wang, Y., 1996. Tectonics of Western Tibet, between the Tarim and the Indus. Earth and Planetary Science Letters 142, 311–330.
Mattern, F., Schneider, W., 2000. Suturing of the Proto- and Paleo-Tethys oceans in the western Kunlun (Xinjiang, China). Journal of Asian Earth Sciences 18, 637–650.
Miller, C.F., Miller, J.S., Faulds, J.E., Stevens, C., Cooper, C., 2005. Miocene volcano–plutonic systems, southern Nevada: A window into upper crustal magmatic processes. In: Stevens, C., Cooper, C. (Eds.), Western Great Basin Geology: Fieldtrip Guidebook and Volume, 99. GSA Cordilleran Section, Pacific Section SEPM Publications, pp. 37–66.
Moyen, J.F., Janousek, V., Laurent, O., Bachmann, O., Jacob, J.B., Farina, F., Fiannacca, P., Villaros, A., 2021. Crustal melting vs. fractionation of basaltic magmas: part 1, Granites and paradigms. Lithos 402–403, 106291. https://doi.org/10.1016/j.lithos.2021.106291.
Nandedkar, R.H., Ulmer, P., Müntener, O., 2014. Fractional crystallization of primitive, hydrous arc magmas: an experimental study at 0.7 GPa. Contributions to Mineralogy and Petrology 167, 1015.
Pan, Y.S., Wang, Y., 1994. Discovery and evidence of the Fifth Suture Zone of Qinghai–Tibetan Plateau. Acta Geophysica Sinica 37, 241–250 (in Chinese with English abstract).
Rickwood, P.C., 1989. Boundary lines within petrologic diagrams which use oxides of major and minor elements. Lithos 22, 247–263.
Ridolfi, F., Renzulli, A., Puerini, M., 2010. Stability and chemical equilibrium of amphibole in calc-alkaline magmas: an overview, new thermobarometric formulations and application to subduction-related volcanoes. Contributions to Mineralogy and Petrology 160 (1), 45–66.
Schaen, A.J., Cottle, J.M., Singer, B.S., Keller, C.B., Garibaldi, N., 2017. Complementary crystal accumulation and rhyolite melt segregation in a late Miocene Andean pluton. Geology 45, 835–838.
Sun, S.S., McDonough, W.F., 1989. Chemical and isotopic systematics of oceanic basalts: implications for mantle composition and processes. Geological Society - Special Publications 42, 313–345.
Tang, M., Wang, X.-L., Shu, X.-J., Wang, D., Yang, T., Gopon, P., 2014. Hafnium isotopic heterogeneity in zircons from granitic rocks: geochemical evaluation and modeling of “zircon effect” in crustal anatexis. Earth and Planetary Science Letters 389, 188–199. https://doi.org/10.1016/j.epsl.2013.12.036.
Trail, D., Watson, E.B., Tailby, N.D., 2012. Ce and Eu anomalies in zircon as proxies for the oxidation state of magmas. Geochimica et Cosmochimica Acta 97, 70–87.
Wang, J., Hattori, K., Liu, J.G., Song, Y., Gao, Y.B., Zhang, H., 2017. Shoshonitic- and adakitic magmatism of the Early Paleozoic age in the Western Kunlun orogenic belt, NW China: implications for the early evolution of the northwestern Tibetan plateau. Lithos 286–287, 345–362.
Wang, X.L., Wang, D., Du, D.-H., Li, J.Y., 2021. Diversity of granitic rocks constrained by disequilibrium melting and subsequent incremental emplacement and differentiation. Lithos 402–403, 106255. https://doi.org/10.1016/j.lithos.2021.106255.
Watson, E.B., Liang, Y., 1995. A simple model for sector zoning in slowly grown crystals: Implications for growth rate and lattice diffusion, with emphasis on accessory minerals in crustal rocks. American Mineralogist 80, 1179–1187.
Weinberg, R.F., Hasalova, P., 2015. Water-fluxed melting of the continental crust: a review. Lithos 212, 158–188.
Workman, R.K., Hart, S.R., 2005. Major and trace element composition of the depleted MORB mantle (DMM). Earth and Planetary Science Letters 231, 53–72.
Xiao, W.J., Windley, B.F., Liu, D.Y., Jian, P., Liu, C.Z., Yuan, C., Sun, M., 2005. Accretionary tectonics of the Western Kunlun orogen, China: a Paleozoic–Early Mesozoic, longlived active continental margin with implications for the growth of southern Eurasia. Journal of Geology 113, 687–705.
Yan, L.L., He, Z.Y., Beier, C., Klemd, R., 2018. Zircon trace element constrains on the link between volcanism and plutonism in SE China. Lithos 320, 28–34.
Yan, L.L., He, Z.Y., Klemd, R., Beier, C., Xu, X.S., 2020. Tracking crystal-melt segregation and magma recharge using zircon trace element data. Chemical Geology 542, 119596.
Yuan, C., Sun, M., Zhou, M.F., Zhou, H., Xiao, W.J., Li, J.L., 2002. Tectonic evolution of the West Kunlun: geochronologic and geochemical constraints from Kudi Granitoids. International Geology Review 44, 653–669.
Yuan, C., Sun, M., Zhou, M.F., Xiao, W.J., Zhou, H., 2005. Geochemistry and petrogenesis of the Yishak Volcanic Sequence, Kudi ophiolite, West Kunlun (NW China): implications for the magmatic evolution in a subduction zone environment. Contributions to Mineralogy and Petrology 150, 195–211.
Zhang, C.L., Yu, H.F., Ye, H.M., Zhao, Y., Zhang, D.S., 2006. Aoyitake plagiogranite in western Tarim Block, NW China: age, geochemistry, petrogenesis and its tectonic implications. Science in China Series D: Earth Sciences 36 (10), 881–893.
Zhang, Y., Niu, Y.L., Hu, Y., Liu, J.J., Ye, L., Kong, J.J., Duan, M., 2016. The syncollisional granitoid magmatism and continental crust growth in the West Kunlun Orogen, China–evidence from geochronology and geochemistry of the Arkarz pluton. Lithos 245, 191–204.
Zhang, C.L., Zou, H.B., Ye, X.T., Chen, X.Y., 2019. Tectonic evolution of the West Kunlun Orogenic Belt along the northern margin of the Tibetan Plateau: implications for the assembly of the Tarim terrane to Gondwana. Geoscience Frontiers 10, 973–988. https://doi.org/10.1016/j.gsf.2018.05.006.3.
Zou, X.Y., Jiang, J.L., Qin, K.Z., Zhang, Y.G., Yang, W., Li, X.H., 2021. Progress in the principle and application of zircon trace element. Acta Petrologica Sinica 37 (4), 985–999. https://doi.org/10.18654/1000-0569/2021.04.03.